JGR Space Physics

RESEARCH ARTICLE
10.1029/2024JA033254

Piercing the Martian Veil: A Statistical Study of Interplanetary Magnetic Field Reach Through Ionospheric Pressure Balance

S. R. Shaver[1], L. Andersson[1], R. Ramstad[1], Bhagyashree Waghule[2], D. Brain[1], R. Lillis[3], T. Cravens[4], J. Halekas[5], S. Xu[3], P. C. Hinton[1], D. Malaspina[1], M. W. Liemohn[6], S. Ledvina[3], J. R. Gruesbeck[7,8], and S. Curry[1]

[1]Laboratory for Atmospheric and Space Physics, University of Colorado, Boulder, CO, USA, [2]University of Colorado Boulder, Boulder, CO, USA, [3]Space Sciences Laboratory, University of California Berkeley, Berkeley, CA, USA, [4]Department of Physics and Astronomy, University of Kansas, Lawrence, KS, USA, [5]Department of Physics and Astronomy, University of Iowa, Iowa City, IA, USA, [6]Department of Climate and Space Sciences and Engineering, University of Michigan, Ann Arbor, MI, USA, [7]Department of Astronomy, University of Maryland, College Park, MD, USA, [8]Solar System Exploration Division, NASA Goddard Space Flight Center, Greenbelt, MD, USA

Abstract Mars, being a small planet with a tenuous atmosphere, does not have a sharp boundary between regions dominated by solar wind plasma and planetary plasma. Instead, this transition is typically extended, allowing the interplanetary magnetic field (IMF) to penetrate into the Martian ionosphere. However, the depth of this penetration is not well understood. Using 6 years of MAVEN data, we statistically assess locations where a transition exists between the dominance of magnetic versus cold (<1 eV), thermal plasma pressure to better understand the reach of the IMF. We identify the presence or absence of pressure transitions from 200 to 800 km altitude for each MAVEN orbit and find a clear transition in ∼55% of cases. The pressure transition locations are mapped in different coordinate systems that provide insight into the solar and planetary driving conditions that cause a detected transition region. Transitions are more likely to occur under weak-to-nominal solar wind conditions, away from strong crustal magnetic fields, near the terminator, on the dusk side of the planet compared to the dawn side, and in the negative solar wind motional electric field hemisphere. We speculate on possible causes for asymmetries that arise in the mapped locations of these pressure transitions and the effect that penetrated IMF may have on driving plasma dynamics in the Martian ionosphere.

Plain Language Summary The Sun emits a constant stream of charged particles known as the solar wind. These particles carry a magnetic field as they move through the solar system. When sunlight hits the thin atmosphere of Mars, it causes the atmospheric particles to become electrically charged, creating the Martian ionosphere. When the solar wind interacts with the Martian ionosphere, it causes currents to flow that divert the solar wind particles around Mars. However, the magnetic field carried by the solar wind can penetrate further into the Martian atmosphere, leading to mass, momentum, and energy exchange between the solar wind and the planet's atmosphere. To better understand the penetration of the solar wind's magnetic field into the Martian atmosphere, we study locations where magnetic pressure and thermal ionospheric pressure are balanced. These locations are assumed to mark the transition between a region where the penetrated solar magnetic field drives plasma motion, to a region where the motions of Martian ionospheric particles dominate plasma dynamics. This will help future studies determine how far into the atmosphere electromagnetic forces can drive dynamics.

Key Points:

- Pressure transitions between 200 and 800 km are only observed on roughly 55% of the orbits studied
- Pressure transitions are dominantly absent over strong crustal magnetic fields in the region studied
- Occurrence increases under weak-to-nominal solar wind conditions, on the dusk side, and in the negative motional electric field hemisphere

Correspondence to:
S. R. Shaver,
skylar.shaver@lasp.colorado.edu

Citation:
Shaver, S. R., Andersson, L., Ramstad, R., Waghule, B., Brain, D., Lillis, R., et al. (2025). Piercing the Martian veil: A statistical study of interplanetary magnetic field reach through ionospheric pressure balance. *Journal of Geophysical Research: Space Physics*, *130*, e2024JA033254. https://doi.org/10.1029/2024JA033254

Received 3 SEP 2024
Accepted 10 JAN 2025

Author Contributions:
Conceptualization: L. Andersson, R. Ramstad, D. Brain, T. Cravens, D. Malaspina, M. W. Liemohn, S. Ledvina
Data curation: L. Andersson, R. Ramstad, J. Halekas, J. R. Gruesbeck, S. Curry
Funding acquisition: S. Curry
Methodology: L. Andersson
Resources: R. Ramstad
Software: L. Andersson, R. Lillis, J. Halekas
Supervision: L. Andersson
Validation: L. Andersson
Writing – original draft: L. Andersson, D. Malaspina
Writing – review & editing: L. Andersson, R. Ramstad, Bhagyashree Waghule, D. Brain, R. Lillis, T. Cravens, J. Halekas, S. Xu, P. C. Hinton, D. Malaspina, M. W. Liemohn, S. Ledvina

©2025. The Author(s).
This is an open access article under the terms of the Creative Commons Attribution License, which permits use, distribution and reproduction in any medium, provided the original work is properly cited.

1. Introduction

Mars, with its small size, tenuous atmosphere, and localized intrinsic magnetic fields, represents a unique plasma laboratory in our solar system through its interaction with the solar wind. The solar wind consists of ionized particles moving through interplanetary space that carry the interplanetary magnetic field (IMF). When the supersonic solar wind encounters a conductive obstacle such as the dayside ionosphere of Mars, a bow shock is formed where the solar wind particles are slowed below magnetosonic speeds, thermalized, and thereafter diverted around the planet. Near this stagnation point, mass-loading and induced ionospheric currents cause the IMF to pile-up on the dayside and drape around the planet (Baumjohann et al., 2010; Ramstad et al., 2020; Szegö et al., 2000). The associated magnetic field enhancement creates the Martian "induced magnetosphere" and what is known as the induced magnetosphere boundary (IMB) between the shocked solar wind and the planetary

ionosphere (see, for example, Luhmann et al. (2004); Bertucci et al. (2011) and references therein). The solar wind particles are mostly diverted around the planet at this location; however, the IMF can penetrate deeper than this stagnation point into the Martian ionosphere (Dong et al., 2019). The depth at which the IMF can reach within the ionosphere is not well understood, and has been an ongoing quest for nonintrinsic planets (Moses et al., 1988; Slavin & Holzer, 1982).

The lowest altitude that the IMF can penetrate into the ionosphere of an induced magnetosphere system has been thought to be where the magnetic pressure is balanced by ionospheric thermal plasma pressure. This thought arises from the MHD momentum equation under the assumptions that (a) the plasma is nearly stationary ($\mathbf{u} = \mathbf{0}$) at the pressure balance location, (b) gravity can be neglected, (c) the magnetic geometry is planar (i.e., the magnetic field lines are straight), which leads to conditions where the combination of thermal plasma pressure and magnetic pressure is constant in the direction normal to the magnetic field (see e.g. Cravens (1997)). With these assumptions in mind, the depth that the IMF can reach within a planetary ionosphere can be evaluated by examining pressure balance locations. The sharp Venusian ionopause, observed during solar maximum, under low solar wind dynamic pressure compared to ionospheric thermal pressure, and in the positive solar wind motional electric field hemisphere, represents a clear example of this static force balance (Luhmann & Cravens, 1991; Zhang et al., 2010). Here, a thin current layer separates the solar wind plasma and IMF at higher altitudes from the planetary ionospheric plasma at lower altitudes (Cravens, 1997).

When the planetary system changes and the above assumptions are broken, the location where these two pressures are equal will not generally represent the stagnation point of the IMF. This is often the case within the Martian system, which has a complex magnetosphere (see e.g. Nagy et al. (2004) and references therein). While original definitions of the Martian "ionopause" referred to a pressure balance (Cloutier & Daniell, 1973; Spreiter et al., 1970), the term has since taken on many meanings. Recent definitions include the location where there is a steep gradient in the thermal electron density (Chu et al., 2019; Duru et al., 2009), a steep gradient in ion density (Vogt et al., 2015), or where the thermal electron density falls below a specific threshold (Han et al., 2014). Other studies have defined the Martian ionopause as a pressure balance between the solar wind dynamic pressure, magnetic pressure, and thermal ionospheric and/or sheath plasma pressures or a combination of classification criteria (Cloutier & Daniell, 1973; Mendillo et al., 2017; Sánchez-Cano et al., 2020). To reduce confusion, we have chosen not to use the term "ionopause" in this study to define regions of pressure balance between magnetic and ionospheric thermal pressure in the Martian ionosphere.

The location of the lower transition from magnetic to ionospheric thermal pressure dominance depends on solar wind conditions and the structure of the planetary magnetosphere (Holmberg et al., 2019). As the solar wind interacts with the Martian induced magnetosphere, solar wind dynamic pressure is converted to thermal pressure below the bowshock within the sheath, which is then converted to magnetic pressure within the pile-up region, then back to thermal plasma pressure within the cold ionosphere (Crider et al., 2002; Ma et al., 2004). Measurements made by the Mars Atmosphere and Volatile EvolutioN (MAVEN) mission (Jakosky et al., 2015) provide means for a comprehensive analysis of the lower pressure balance location, which was previously found near an altitude of roughly 300 km (Holmberg et al., 2019). At ∼300 km, the magnetic field strength is stronger on the planet's dayside in the pile-up region and decreases on the nightside; however, there is no clear gradient in the electron density or pressure with increasing SZA (Hamil et al., 2019). Furthermore, electron temperatures increase with increasing altitude, whereas the density decreases (see, e.g., Schunk & Nagy, 2009). These typical conditions prime the system for the interaction between flux tubes and the Martian ionosphere.

In this work, any mention of "flux tube" is meant in reference to the IMF, although magnetic structures can arise from other sources within the Martian ionosphere (Cravens et al., 2023; Hamil et al., 2022). These structures, such as the IMF, induced ionospheric currents, and crustal magnetic fields, may all contribute to the calculated magnetic pressure. Mars' crustal magnetic fields are localized regions of magnetic fields remnant from a time when the planet had an internal dynamo that magnetized the planet's crust (see Nagy et al. (2004) or Connerney et al. (2004) and references therein). The strongest crustal fields reside mainly in the southern hemisphere of the planet between 120° and 240° longitude [international astronomical units], so that Mars shows a constantly changing magnetic "face" to the solar wind as the planet rotates daily and tilts with season (Gao et al., 2021; Langlais et al., 2004, 2019). This produces the "hybrid magnetosphere" of Mars, which has both direct Venus-like induced magnetosphere and Earth-like intrinsic field interactions between the solar wind and the planetary system (Brain et al., 2017). Although the influence of crustal magnetic fields is not explicitly removed from this study, we

find that the lower pressure balance does not tend to occur over strong crustal magnetic fields. Therefore, we assume these locations result from the interaction of a flux tube with the Martian ionosphere.

The balance between magnetic and cold thermal plasma pressure at Mars is a dynamic transition region with a complex morphology (Mitchell et al., 2001). Studies of pressure transitions have been confined to manual identification techniques or focused on a localized region (Holmberg et al., 2019; Sánchez-Cano et al., 2020). Hamil et al. (2019) showed that the plasma beta above roughly 200 km at Mars is typically less than one at all SZAs, indicating the dominance of magnetic pressure. The present study is a statistical analysis of pressure balance spanning 6 years of MAVEN data to determine the relationship between solar wind driving conditions and where a pressure transition is most likely to occur. Here, we use an algorithm that automatically identifies locations of pressure balance between 200 and 800 km in altitude around Mars. The resulting data set is analyzed to understand how deep in the Martian ionosphere the IMF influences the dynamics.

This paper is structured in the following way: first, the methods, data sets used, and assumptions made for the identification of regions of balance between magnetic and thermal plasma pressure are described in Section 2. In Section 3, this data set is used to statistically identify which upstream solar wind and IMF parameters lead to an identified pressure transition. These locations are also mapped in areographic coordinates to determine the role of crustal magnetic fields in the identification (or lack thereof) of a pressure balance region. In Section 4, the locations of these plasma transitions are mapped in local time and in different coordinate systems that describe solar conditions to identify trends in the interaction between the IMF and planetary ionosphere. We speculate on one possible scenario governing these interactions in Section 4.3. A conclusion and summary of the findings on these pressure transition locations are finally put forward in Section 5.

2. Methods, Data Sets, and Assumptions

This study investigates the locations of transitions between magnetic and thermal pressure to identify how far down in the Martian ionosphere the IMF influence reaches. The automatic identification of pressure transitions permits a statistical study of the locations of the pressure transition regions relative to different driving processes. Such a statistical study takes advantage of the multiple years of MAVEN data, which has been in orbit around Mars with a comprehensive plasma and neutral instrument suite since 2014 (Jakosky et al., 2015).

In the work presented here, pressure balance regions are determined along each inbound and outbound MAVEN orbit segment between 200 and 800 km in altitude by identifying locations where there is a transition in the dominant plasma pressure. This altitude range was used to search above the neutral collision-dominated region of the ionosphere near 160–200 km ((Akbari et al., 2019; Lillis et al., 2019)) and below the magnetic pileup boundary 600–800 km (Bertucci et al., 2005; Vignes et al., 2000). This altitude range allows the study of pressure balance locations in regions where plasma beta is usually below one and where interactions with neutrals can be neglected (Hamil et al., 2019).

The magnetic pressure $\left(P_B = B^2/2\mu_0\right)$ was determined using magnetic field measurements from the MAG instrument (Connerney et al., 2015). MAG measures the ambient magnetic field strength and direction in three spatial dimensions. For this analysis, the MAG 1-s data product is used. Contributions to the magnetic field strength and, therefore, magnetic pressure may result from the draped IMF, crustal fields, and induced magnetic fields within the Martian ionosphere. Any analysis done pertaining to the Martian crustal fields uses the model by Langlais et al. (2019).

Thermal pressure of cold plasma is used to assess populations and dynamics within the planetary ionosphere. To derive the cold thermal plasma pressure, measurements from the Langmuir Probe and Waves (LPW) instrument are used. Quasi-neutral conditions are assumed ($n_e \sim n_i$, where n_e, n_i describes the bulk electron and ion density). Furthermore, ion and electron temperatures are assumed to be equal for the bulk plasma in the ionosphere $\left(T_e \sim T_i\right)$ in the 200–800 km altitude range used in this investigation (Chen et al., 1978; Chu et al., 2021; Holmberg et al., 2019; Sakai et al., 2016). This altitude range is located above the usual exobase such that interactions with the neutral atmosphere can be ignored. The cold, thermal plasma pressure can therefore be calculated from MAVEN LPW data using $P_{th} = n_e k_b T_e + n_i k_b T_i \simeq 2 n_e k_b T_e$. LPW consists of two sensors that measured n_e and T_e at the beginning of the mission. Later in the mission, only Boom 1 was continuously used, and therefore, this study uses only Boom 1 data. The cadence of LPW measurements occurs in multiples of 4 s. To match the 1-s cadence of MAG, each second of an LPW voltage sweep was assigned the resulting plasma

measurement throughout that sweep time. To maintain confidence in the accuracy of these measurements, we only include electron densities greater than 100 cm^{-3} and temperatures greater than 500 K (Andersson et al., 2015). The electron density is usually low near 800 km altitude and this might influence the result of this study based on the criteria described below.

In order to account for observation biases and to investigate the region between the shocked solar wind and planetary ionosphere, the following conditions were imposed in the search for pressure balance regions along inbound and outbound orbit segments: First, the data set was limited to orbits between January 2015 through February 2021, in order to study solar minimum conditions. Second, the orbits studied had to have LPW measurements at both the lower altitudes (200–250 km) and upper altitudes (750–800 km) used in this study. The LPW instrument, used to measure electron density and temperatures, is optimally designed for a high-density ionospheric plasma environment (i.e., a cold population). The imposed caveat that LPW data be available between 750 and 800 km along "viable" orbits may have implications for any interpretations of the findings, such as filtering for conditions when cold plasma populations dominate at the highest altitudes studied here. Furthermore, this work assumes that the resulting altitude profiles represent the vertical structure of the plasma environment. However, as the spacecraft approaches the lower altitudes used in this study, the trajectory may represent more horizontal motion relative to the planet than vertical. This assumption may influence the resulting analysis surrounding the existence of the transition regions. For example, multiple transitions may be detected as the spacecraft "skims" the boundary region. However, the focus of this study is to statistically map the locations of pressure balance relative to solar parameters to determine the configuration of the penetrated IMF. Therefore, skimming the boundary surface in multiple locations ultimately helps produce an image of the boundary configuration.

With these assumptions in mind, an algorithm was then developed to automatically identify transitions in the dominant plasma pressure (i.e., pressure balance regions) along orbit segments. Because the Martian ionosphere is dynamic, the pressure identification algorithm must account for any biases due to particle motions, spacecraft trajectory, or instrumental errors. Therefore, by requiring a larger region to denote a transition, the identification of these pressure transition regions is more likely to be statistically sound. The detection algorithm accounts for these biases using the following approaches: (a) transitions detected within one data point of the previous transition are removed, and (b) either pressure must be 20% greater in magnitude than the other to be considered dominant. This allows an altitude *region* to be demarcated as the location of pressure balance that can vary. These altitude regions were not permitted to exceed a total 50 km in vertical distance. When one point location is referred to in this study, it represents the median location between the designated start and end locations of an automatically identified pressure balance region.

This work conducts a statistical analysis on the locations of the determined pressure transition regions. Example magnetic and thermal plasma pressure altitude profiles and the identification of transitions are shown in Figure 1. In this Figure, magnetic pressure is shown in pink and bulk thermal plasma pressure in purple. The detected transition regions are highlighted by horizontal orange bars. Panel (a) depicts an inbound orbit segment where no pressure transitions were detected. Panel (b) depicts an outbound orbit segment with one transition detected, panel (c) with two transitions, and panel (d) an inbound segment with three transitions detected along the orbit segment between 200 and 800 km in altitude. Often, when the algorithm identified a transition along an orbit segment, multiple transition detections were recorded. This could suggest variations in the Martian-induced magnetosphere's characteristics. How each transition is treated in the following investigations is described in the corresponding section of the paper.

When evaluating all viable orbits, magnetic pressure, as opposed to thermal pressure, dominates at high altitudes for over 90% of the orbits studied. Magnetic pressure is expected to dominate within the magnetic pile-up region, which typically exists between ~650–800 km altitude at low SZA (Acuña et al., 1998; Breus et al., 1991; Holmberg et al., 2019; Matsunaga et al., 2017; Trotignon et al., 2006; Vignes et al., 2000). The orbit segments with thermal plasma pressure dominant at the higher altitudes were mainly found on the nightside of the planet. These orbits are disregarded as they likely do not represent the interaction of the ionosphere with the draped IMF, and this helps remove orbits where thermal pressure within the magnetosheath may play a significant role at the altitudes studied.

In order to determine the influence of upstream solar wind conditions, which is studied in Sections 3.1 and 4.2, solar wind densities, velocities, magnetic field strength and direction were derived using upstream conditions

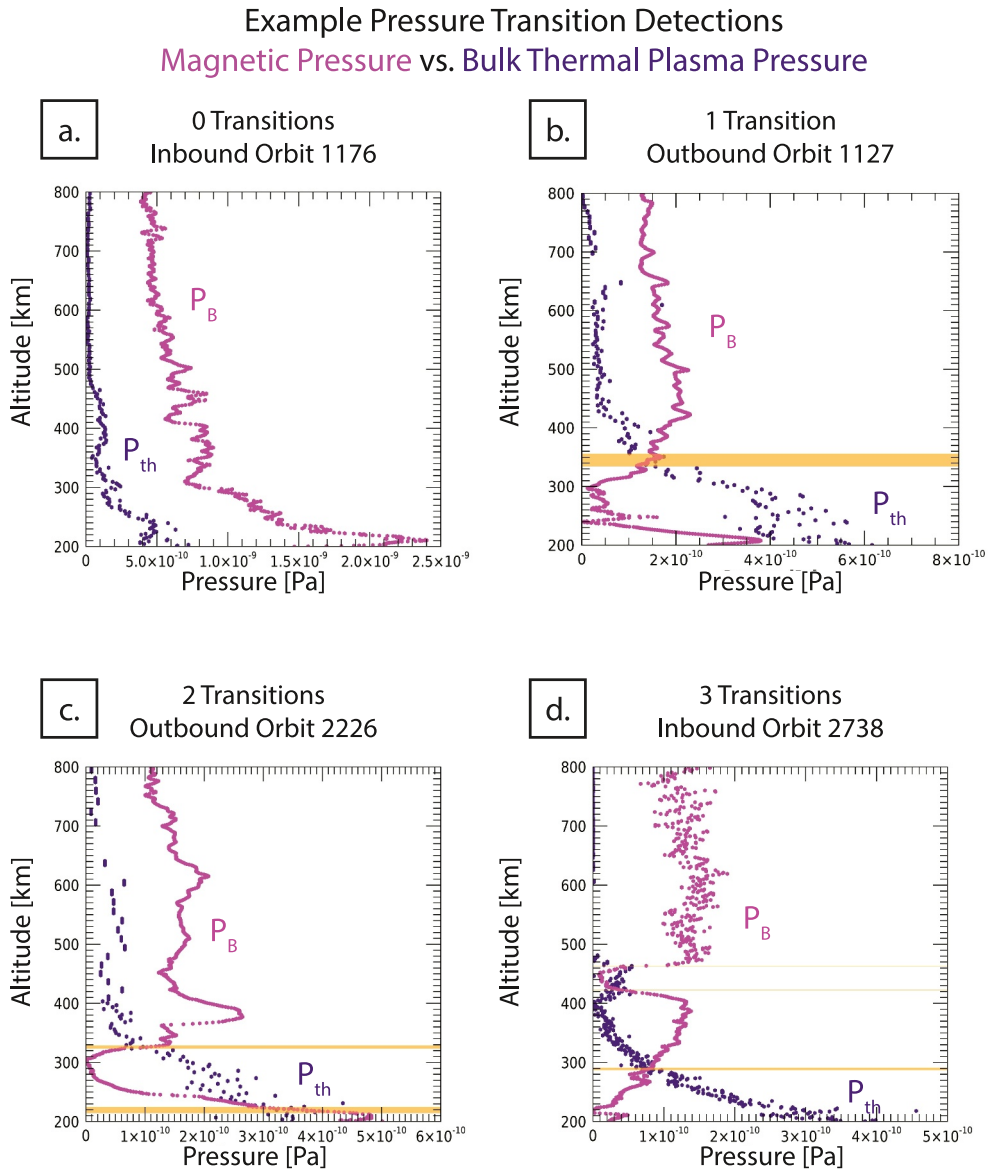


Figure 1. Example altitude profiles of magnetic (pink) and cold, thermal plasma pressure (purple) and the corresponding detection of transitions in the dominant pressure, or pressure balance regions (orange horizontal lines). The thickness of the orange horizontal lines represents the thickness in altitude of the identified pressure balance regions. The selected orbits represent 0, 1, 2, and 3 transitions within the altitude region of interest. Roughly 45% of the orbits analyzed had no transitions detected between 200 and 800 km, like that shown in panel a of this figure.

provided using the method of J. S. Halekas et al. (2017). The precession of MAVEN's orbit does not allow continuous sampling of upstream conditions. Therefore, to analyze the influence of upstream conditions, we only use orbits with solar wind parameters available near apoapsis. This manuscript uses solar wind values closest in time to a determined pressure transition along an orbit segment.

Solar EUV radiation estimates are used to determine the effect of irradiance on the presence of an observed pressure balance location. Solar ionizing irradiance (0–91 nm) is derived from the MAVEN Extreme Ultra-Violet Monitor (EUVM) Level 3 (L3) FISM-M empirical model (Thiemann et al., 2017). Only solar irradiance estimates made within one day of an analyzed location were used in this study.

The number of orbits used in each investigation of this study changes with their respective constraints. Table 1 provides the number of orbit segments used for each statistical analysis conducted in this manuscript under the

Table 1
The Number of Orbit Segments Used in the Different Investigations of This Manuscript

The databases for different constraints	Number of orbit segments
Total Orbits January 2015–February 2021	24,859
Viable Orbits	14,956
Viable Orbits with B field Dominant at High Altitudes	14,145
Viable Orbits with Transition Detected	8,049
Orbits with Upstream Solar Wind Measurements	8,035
Orbits with Upstream Solar Wind Measurements and Transition Detected	4,733

different constraining conditions discussed in this section. These data sets are used to analyze the solar drivers that lead to a detected pressure transition region.

In this work, three different coordinate systems are used to describe the influences of solar and Martian surface conditions on pressure transition regions. Mars-Solar-Orbital (MSO) coordinates describe the spacecraft's position relative to Mars and the Sun. Positive X values point from the center of the planet toward the Sun, positive Z values point northward out of Mars' orbital plane about the Sun, and positive Y completes the right-hand system (pointing generally toward dusk). Mars-Solar-Electric (MSE) coordinates are used to assess the relative importance of the solar wind motional electric field ($\mathbf{E}_{mot} = -\mathbf{v}_{SW} \times \mathbf{B}_{IMF}$, where $\mathbf{v}_{SW}$ is the solar wind bulk velocity, and $\mathbf{B}_{IMF}$ is the IMF vector) on driving plasma dynamics. In the MSE coordinate system, positive X is directed opposite to the bulk solar wind velocity, positive Z points along the solar wind motional electric field, and the Y axis completes the right-hand system (pointing in the direction of the projection of the IMF vector into the MSE XZ plane). The International Astronomical Units body (IAU) coordinate system (which rotates with the solid planet) was also used to map the location of pressure transition relative to surface features on Mars, with a specific focus on whether transitions were found over regions of strong crustal magnetic fields.

3. Conditions Leading to an Observed Pressure Transition

3.1. Upstream Drivers Influence on Transition Occurrence

The first investigation of this data set aims to identify which solar wind conditions lead to the detection of a pressure transition within the studied altitude region. To achieve this, we compare the solar wind and IMF parameters of orbits with identified pressure transitions to those without. This comparison uses the 8035 viable orbit segments with available upstream solar wind parameters (see Table 1). We expected to observe a pressure transition along most, if not all, orbits, as the spacecraft moves from the magnetic pileup region into the Martian ionosphere (see the introduction for further discussion). However, only ∼60% of the 8035 orbit segments had a detected pressure balance region within the Martian magnetosphere.

The solar wind density, speed, IMF magnitude, motional electric field, solar wind dynamic pressure, and solar EUV irradiance were evaluated for orbits with and without transitions in pressure detected.

The results are presented in Figure 2, which depicts histograms of upstream conditions for orbit segments where instances of pressure balance region(s) are observed (shown in blue) or are not observed (shown in red). The solar wind conditions along all orbit segments, normalized to the total number of occurrences, are shown in green at the bottom of each histogram for reference.

Pressure balance tends to occur under weak to nominal solar wind conditions, as can be interpreted from Figure 2. Pressure transitions are more likely to be observed when the solar wind density is less than roughly 5 cm^{-3} (panel a), when the solar wind velocity is below ∼550 km/s (panel b), and when the total IMF strength is below 4 nT (panel c). The solar wind density at Mars is typically between 1 and 4 cm^{-3}, the median solar wind flow speeds are near 350–450 km/s, and the IMF field strength is around 2 nT, which is presented by the green histograms in Figure 2 and is consistent with previous studies (Marquette et al., 2018; J. S. Halekas et al., 2017). The pressure transition boundary is also more likely to be observed in the -Z MSE hemisphere (panel d). In the -Z hemisphere, the motional electric field ($\mathbf{E}_{mot} = -\mathbf{v}_{SW} \times \mathbf{B}_{SW}$) is directed toward the planet, which may affect the resulting penetration of the IMF into the Martian ionosphere. The implications of the MSE results are further assessed in

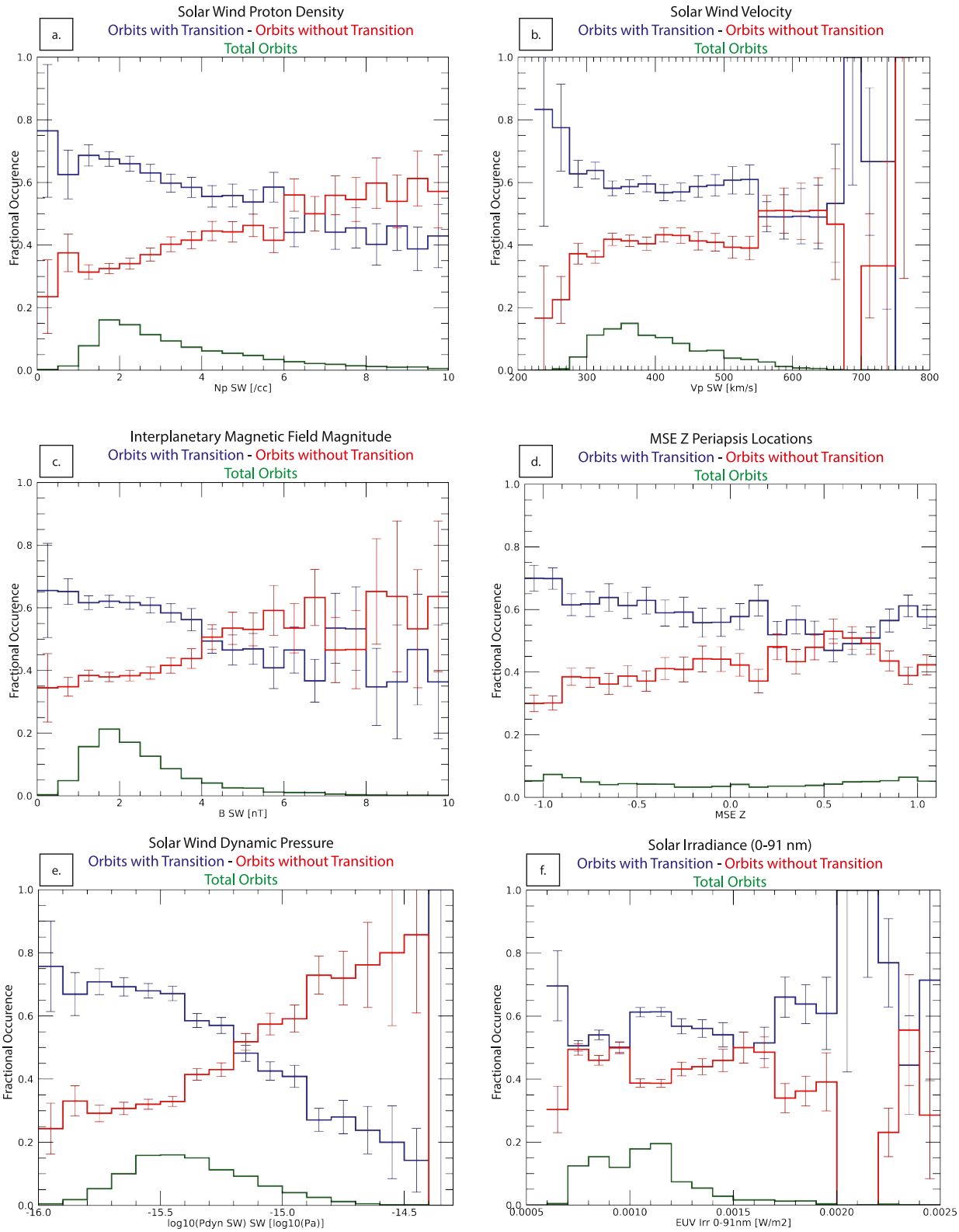

a.
Solar Wind Proton Density
Orbits with Transition - Orbits without Transition
Total Orbits
Fractional Occurence
Np SW [/cc]
b.
Solar Wind Velocity
Orbits with Transition - Orbits without Transition
Total Orbits
Fractional Occurence
Vp SW [km/s]
c.
Interplanetary Magnetic Field Magnitude
Orbits with Transition - Orbits without Transition
Total Orbits
Fractional Occurence
B SW [nT]
d.
MSE Z Periapsis Locations
Orbits with Transition - Orbits without Transition
Total Orbits
Fractional Occurence
MSE Z
e.
Solar Wind Dynamic Pressure
Orbits with Transition - Orbits without Transition
Total Orbits
Fractional Occurence
log10(Pdyn SW) SW [log10(Pa)]
f.
Solar Irradiance (0-91 nm)
Orbits with Transition - Orbits without Transition
Total Orbits
Fractional Occurence
EUV Irr 0-91nm [W/m2]

Figure 2.

Section 4 of this paper. Locations of pressure balance are also more likely to be found when the solar wind dynamic pressure is weak to nominal (panel e).

Panel (f) shows that more orbits will have a pressure transition detected than not; however, there is no obvious trend in observations of pressure balance with different ionizing EUV irradiance. One might expect more pressure balance detections with increased EUV due to thermospheric heating and expansion. However, the effect of EUV irradiance is secondary to the influence of solar zenith angle (SZA) on scale height, and it does not impact electron temperatures in the afternoon, when pressure balance regions are most frequently observed (M. Pilinski et al., 2019). This lack of trend with EUV irradiance is reflected in Figure 2f, which includes all SZAs. A more detailed discussion of the relationship between pressure balance regions and SZA is provided in Section 4.1.

Fewer locations of pressure balance are observed along orbits with strong solar wind conditions (Figure 2). This may be due to the strict altitude range of 200–800 km used in this study. The Martian magnetospheric system can expand under lower solar wind dynamic pressure and/or lower magnetic pressure from the pile-up of IMF on the dayside (see e.g. Dubinin, Fraenz, et al., 2019; J. S. Halekas et al., 2023; Shaver et al., 2024). These conditions may, therefore, allow the pressure balance location to rise above 200 km. Conversely, stronger solar wind drivers will compress the ionosphere (Girazian et al., 2019), such that the location where the pressure transition occurs is pushed below the 200 km lower altitude used in this study. Weak solar wind may provide the conditions for the pressure balance investigated in this study to be observed within the designated altitude range (Cloutier & Daniell, 1973; Fowler et al., 2024); this is like the boundary found at Venus above the ion demagnetization altitude (Luhmann & Cravens, 1991).

3.2. Crustal Magnetic Field Influence on Transition Occurrence

The crustal magnetic fields may also influence the altitude that the IMF can reach within the Martian ionosphere. The influence of crustal fields along viable orbits with magnetic pressure dominating at high altitudes (14,145 orbit segments) is therefore analyzed here. Figure 3 depicts maps of the occurrences (or lack thereof) of transitions in dominant plasma pressure in areographic latitude and longitude. Panel (a) shows a 2D histogram map of where transitions in dominant plasma pressure occur relative to the Martian surface. Panel (b) depicts the periapsis location of orbits without an observed transition in dominant plasma pressure (i.e., where magnetic pressure dominates throughout the 200–800 km altitude range studied). Each of these bins spans 10° in both latitude and longitude. Overlayed on the histograms are contours representing the location of crustal fields with a radial component that exceeds 10 nT (Langlais et al., 2019).

Pressure transitions tend not to occur over the crustal magnetic fields within the altitude range evaluated, shown in Figure 3a. Orbits where no transition detected are more likely to approach periapsis near the strong crustal fields (panel b). The lack of an observed transition is likely caused by the contribution of crustal magnetic fields causing the total magnetic pressure (from IMF, induced currents, crustal fields, etc.) to exceed thermal plasma pressure throughout the 200–800 km altitude range. These results indicate that thermal plasma pressure does not control the interaction of the IMF with the Martian system in these areas. Instead, the crustal magnetic fields in these regions are likely the main source responsible for standing off the incoming IMF and a significant contribution to the overall magnetic pressure term, which is consistent with previous studies (Brain et al., 2003; Dubinin, Fraenz, et al., 2019; Ma et al., 2014).

4. Asymmetries in the Observed Pressure Transitions

4.1. Dawn-Dusk Asymmetries in Observed Pressure Transitions

The thermosphere of a rotating planet will be inflated on the planet's dusk side relative to its dawn side because the atmosphere heats and expands as it rotates from dawn to dusk (Bougher et al., 1999; M. Pilinski et al., 2019; Jain

Figure 2. Histograms depicting the upstream driving conditions for orbit segments with (blue) and without (red) observed transitions in the pressure balance. The total normalized solar wind conditions for orbits with solar wind observations are shown in green at the bottom of each histogram for reference. Panel (a) depicts the solar wind proton density for orbits with or without a pressure transition, panel (b) the solar wind proton velocity, panel (c) the upstream IMF strength, panel (d) the Z MSE location of periapsis relative to upstream IMF orientation, panel (e) is the solar wind dynamic pressure, and panel (f) is the modeled EUV irradiance between 0 and 91 nm. The error bars indicate Poisson statistical error based on the number of orbit segments in each bin. Each bin has been normalized by the total number of viable orbits within a bin to provide the percent occurrence.

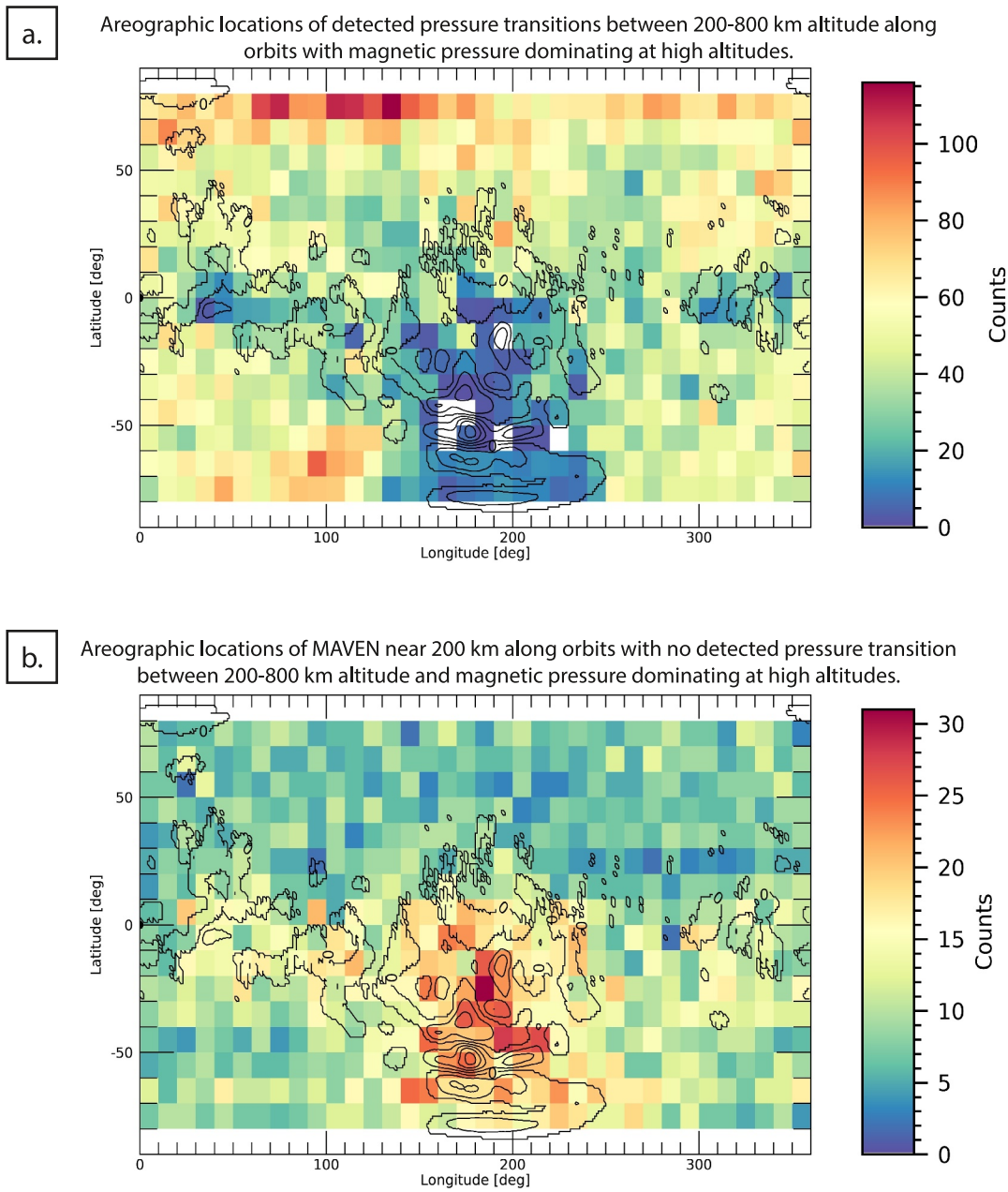


Figure 3. Figures depicting transition dependence on latitude and longitude [IAU] at Mars using 2D histograms to map the spacecraft position under particular conditions. Red colors indicate more occurrences within a specific latitude-longitude bin. Panel (a) shows where pressure transitions occur, panel (b) shows the location of MAVEN's periapsis along orbits where no pressure transition was detected.

et al., 2023). Since the pressure transitions are assumed to mark the interface between the penetrated IMF and planetary ionosphere, their locations should reflect both the draped field configuration and asymmetries between the dawn and dusk side of the planet. Here, the altitudes and local times of the observed pressure transition regions are evaluated to determine whether these signatures are reflected in the data set.

The locations of pressure balance along orbits with magnetic pressure dominating at high altitudes (8049 orbit segments) are mapped as a function of altitude and MSO local time in Figure 4 to examine the local time dependencies of the transition regions. Panel (a) of Figure 4 is a 2D histogram of all MSO local times visited by

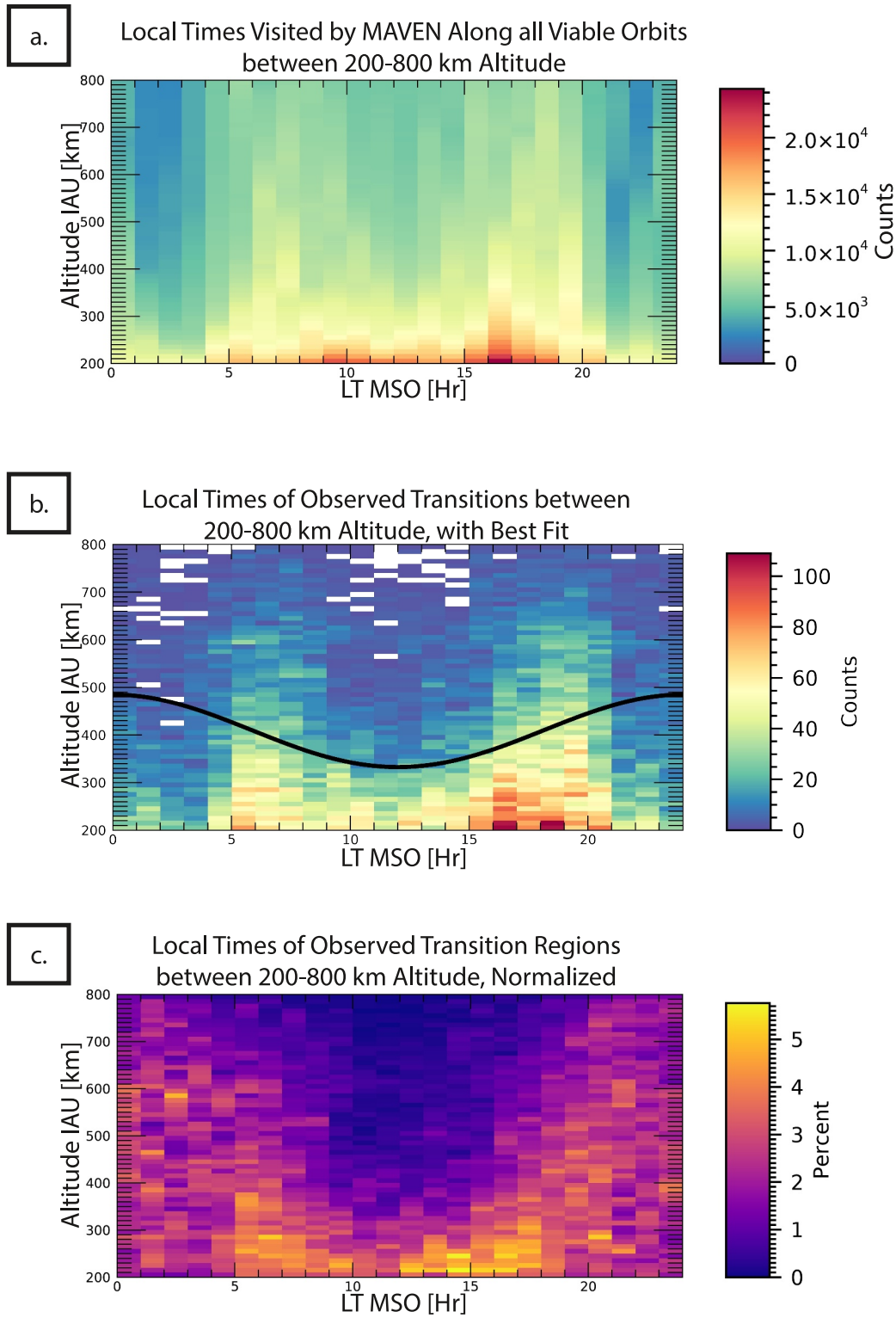


Figure 4. 2D histograms depicting 1-hr local time and 10 km altitude bins of MAVEN and observed transitions locations. Panel (a) are the locations visited by MAVEN along viable orbits used in this study. Panel (b) are the locations of observed pressure balance using the median location of a pressure transition region. Overlayed on panel (b) as a thick black line is the MSO cylindrical fit of the conic section that describes the observed pressure balance locations. This fit is symmetric about 12 LT. Panel (c) are the locations of pressure balance normalized to all locations visited by MAVEN.

MAVEN between 200 and 800 km along viable orbits with magnetic pressure dominating at high altitudes (14,145 orbit segments). Panel (b) shows a 2D histogram of pressure balance locations using the median location of a designated pressure transition region. Panel (c) shows the full designated pressure transition regions normalized to panel (a).

Previous studies have modeled a few of the different boundary regions of the Martian induced magnetosphere using curve fitting techniques (Slavin & Holzer, 1981; Trotignon et al., 2006; Vignes et al., 2000). A similar empirical model for pressure transition locations between magnetic and cold, thermal plasma pressure is derived here and plotted in Figure 4b as a solid black line. The median location of each determined pressure transition region was used to derive a reduced chi-square fit of a conic section in MSO cylindrical coordinates, given by Equation 1, to the pressure balance locations.

$$r = \frac{L}{1 + e\cos\theta} + x_F \tag{1}$$

This equation is used to determine the best fit in (r,θ) polar coordinates, where L is the semi-latus rectum, and e represents the eccentricity of the conic section, and θ is the SZA. A linear regression was then applied to this fit to determine the offset of the conic focus, x_F, along the MSO-X symmetry axis. The best fit of the model was found by searching for the minimum chi-square value of a domain-space of eccentricity values that range from 0.001 to 2 in increments of 0.001, and semi-latus rectum values from 0.01 to 2 in increments of 0.01. The resulting conic fit parameters are given in Table 2. This approach using cylindrical coordinates results in the best fit to the transition region that is symmetric about local noon, which can provide a reference for differences between the dawn and dusk sides of the planet.

Fewer pressure balance locations are found near noon compared to the terminators (6 LT and 18 LT), as shown in Figures 4b and 4c. This is likely due to the compression of the dayside ionosphere, placing the pressure balance region below 200 km in altitude near 12 LT. Between 200 and 800 km, more transitions are found on the dusk side of the planet compared to the dawn side. This may be connected to the rotation of the planet and its atmosphere, which causes the thermosphere to expand on the dusk side compared to the dawn side (Bougher et al., 1999; M. Pilinski et al., 2019; Gupta et al., 2019). Near the dawn and dusk terminators, significant thermospheric temperature and density enhancements due to dynamical effects have been observed (Forbes & Moudden, 2009; M. Pilinski et al., 2018; M. D. Pilinski et al., 2023). These features may play a role in whether pressure balance occurs, but such analysis is left for future studies.

The transition between piled-up and draped IMF and cold, ionospheric plasma is expected to be found at a lower altitude near the subsolar point and a higher altitude at larger SZAs due to the lower radial pressure that permits the IMF to flare at higher SZAs (Cravens et al., 2017; Crider et al., 2003; Hamil et al., 2019). This SZA dependence is observed in the pressure transition locations (Figures 4b and 4c). Transitions are more likely to occur at lower altitudes near 12 LT and at higher altitudes near the terminators. The SZA dependence of observed transitions is evident in the resulting fit (black line in 4b) that varies roughly 200 km in altitude between the subsolar and antisolar locations. We, therefore, assume this reflects the flaring of the draped IMF about the planet.

Interestingly, at both the dawn and dusk terminators, there is a population of transition occurrences near 600 km in altitude (Figure 4b). The ion composition boundary (ICB), which marks the transition between light solar wind ions to heavy planetary ions, has been found to exist near 600 km in previous studies and has previously been associated with another pressure balance location in the Martian system (Holmberg et al., 2019; Xu et al., 2016). The ICB is, on average, where the normal magnetic pressure balances the solar wind ram pressure (J. S. Halekas et al., 2018). While the ICB is typically found at a similar location to the induced magnetosphere boundary (IMB) on the dayside of the planet, the flank and nightside ICB location is variable (J. S. Halekas et al., 2018; Shaver et al., 2024). Toward the nightside, the ICB is generally observed beneath the IMB unless it is located in the southern and -Emot,sw hemisphere (Matsunaga et al., 2017). The statistical study done by Hamil et al. (2019) found no strong gradient in the cold, thermal pressure with SZA, so the observed pressure transitions near 600 km at the terminators may be associated with the ICB. However, we leave further analysis for future studies.

Table 2
Values for Conic Fit of Pressure Balance Boundary, Based on Individual Crossing Occurrences

Parameter	Value
$X_F\,[R_M]$	−0.0024
e	0.02
$L[R_M]$	1.12

4.2. Asymmetries in Solar Driver Influence on Transition Location

To investigate what conditions lead to an observed transition in dominant plasma pressure, the effect of SZA and the solar wind motional electric field are analyzed. By mapping the transition locations in Mars-Solar-Orbital (MSO) and Mars-Solar-Electric (MSE) coordinate systems the influence of these solar drivers on the boundary region formation can be studied. Figure 5 shows 2D histograms of the pressure transition locations in MSO and MSE coordinate frames. Panels a–c of Figure 5 depict the transition locations in MSO coordinates, which describe the spacecraft's position relative to Mars and the Sun. Here, the set of 8049 orbit segments have been used for analysis. The MSO histograms of pressure transition locations have been normalized by the locations visited by MAVEN along all viable orbits with magnetic pressure dominating at high altitudes (14,145 orbit segments). Panels d–f show the locations of the pressure transitions in MSE coordinates along orbits with available upstream solar wind parameters (4733 orbit segments). The MSE histograms have *not* been normalized due to MAVEN's precessing orbit causing a lack of consistent upstream solar wind coverage. However, as indicated by the green lines depicting upstream solar wind measurements of all viable orbits in Figure 2, we assume there is adequate coverage of typical solar wind conditions and configurations. The lack of consistent upstream solar wind sampling likely causes the biasing of the results toward the terminator ($X = 0$) in the MSE view, but we expect there is no bias in the $\pm Z$ MSE pressure transition location dependence. All of the 2D plots shown in Figure 5 have been integrated along the third axis.

Solar irradiance will ionize the neutral atmosphere where induced currents can create a barrier between the ionosphere and penetrating IMF. Solar irradiance is deposited on the dayside of the planet, and is strongest near the subsolar location (Bougher et al., 2017). Panels (a) and (b) show that these transitions are more likely to occur at higher SZAs, and on the dusk side of the planet ($Y_{MSO} > 0$), which is consistent with Figure 4. Panels (b) and (c) show that the pressure transitions are more likely in the Northern hemisphere of the planet ($Z_{MSO} > 0$), which is consistent with Figure 3 as these transitions are not found over the strong crustal magnetic fields in the southern areographic hemisphere.

As previously discussed, the increase in pressure transitions on the dusk side suggests that there may be a connection between the strength of the ionosphere and the depth that the IMF can penetrate. This is expected as longer EUV exposure of the atmosphere as it rotates with the planet from the dawn to dusk side will cause the thermosphere to expand (M. Pilinski et al., 2019). Here, stronger shielding currents may be able to flow between 200 and 800 km in altitude that can stop the IMF from reaching lower altitudes.

What is unexpected is the increased occurrences near the terminator compared to the subsolar location. This may be due to the expected pressure transitions occurring below the lower 200 km altitude cutoff used in this study at lower SZAs. The flaring of the draped IMF at high SZA may allow the ionospheric plasma to expand to higher altitudes, where a transition between the two plasma pressures may then be observed. However, alternative physical processes may also cause the pressure transitions to be biased toward the terminator. For example, a change in the magnetic field topology may provide the conditions for an observed pressure balance location (Xu et al., 2019). Also, previous studies of interactions between the IMF and a planetary ionosphere have shown that magnetic stresses can reach a maximum near the terminator at the $E_{mot,SW}$ poles (Pérez-de Tejada, 1986). Examining the pressure transition regions relative to the $E_{mot,SW}$ poles may provide further insight into which processes lead to an observed pressure transition.

Different plasma dynamics between the solar wind and the Martian system have been shown to exist across the positive and negative $E_{mot,SW}$ hemispheres (Dubinin et al., 1996, 2023). The mapped pressure transition locations shown in panels d–f of Figure 5 hints at asymmetrical interactions between the $\pm E_{mot,SW}$ hemispheres. Most pressure transitions occur in the -X MSE (or $+v_{SW}$) direction, shown in Figure 5d, because the solar wind bulk velocity is directed radially outward from the Sun. Furthermore, the relatively even spread of transition regions along the ± Y MSE axes indicates that they occur both parallel and anti-parallel to the general direction of the IMF. This is consistent with what is expected for draped IMF around the planet. Panels (e) and (f) show that the transitions are more likely to occur in the $-E_{SW}$ hemisphere. Panel (f) shows that pressure transitions occur in multiple locations relative to the general direction of the IMF in the $-E_{SW}$ hemisphere, but occurrences in the $+E_{SW}$ hemisphere are more likely off the pole.

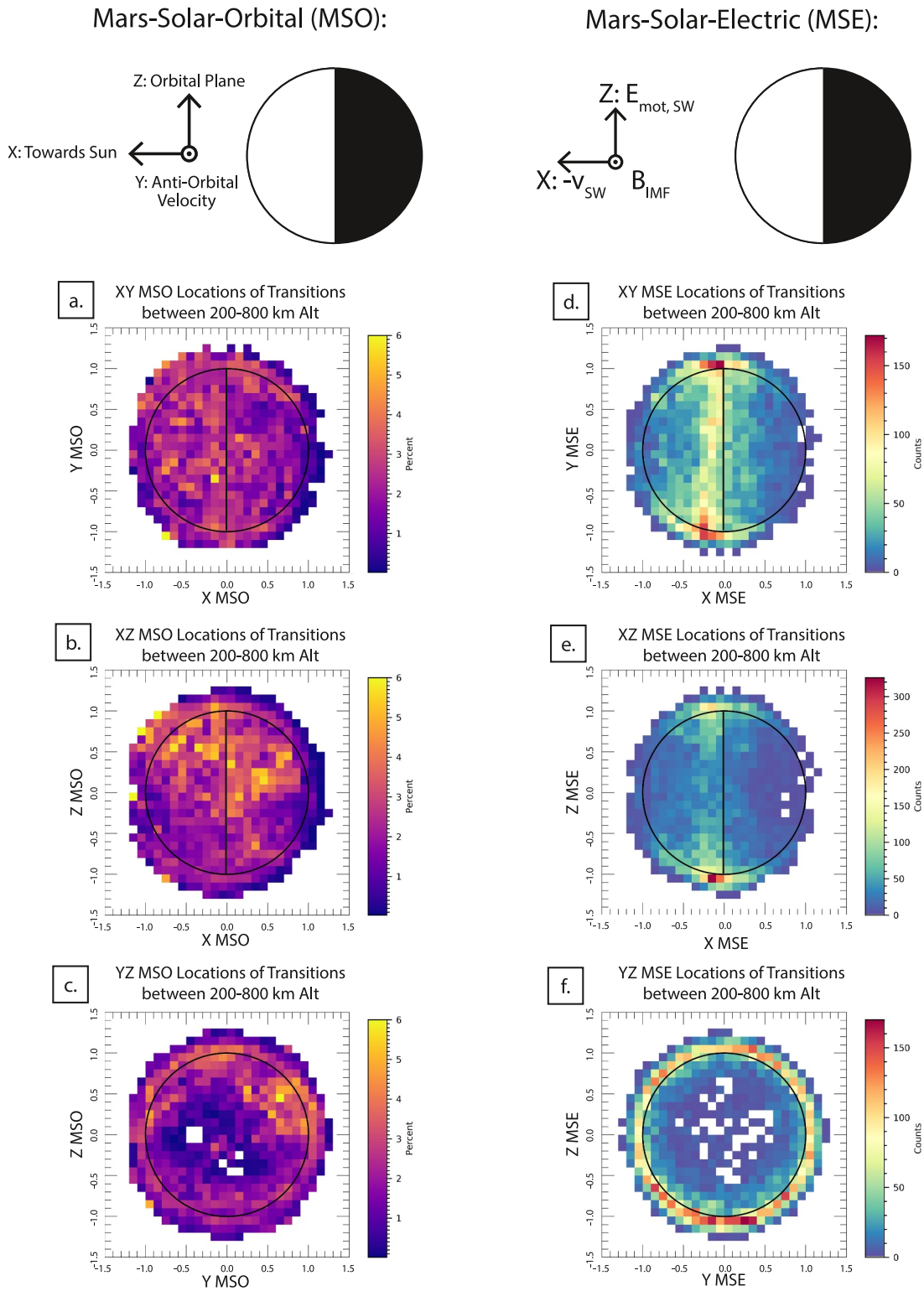


Figure 5. 2D histograms depicting locations of pressure transition regions in MSO (panels a–c) and MSE (panels d–f) coordinate systems in units of Martian radii [R_{Mars}]. The MSO histograms have been normalized to the location of MAVEN along its orbit between 200 and 800 km over the period studied. The MSE histograms have not been normalized because the precession of MAVEN's orbit does not allow the direct sampling of the solar wind at each apoapsis.

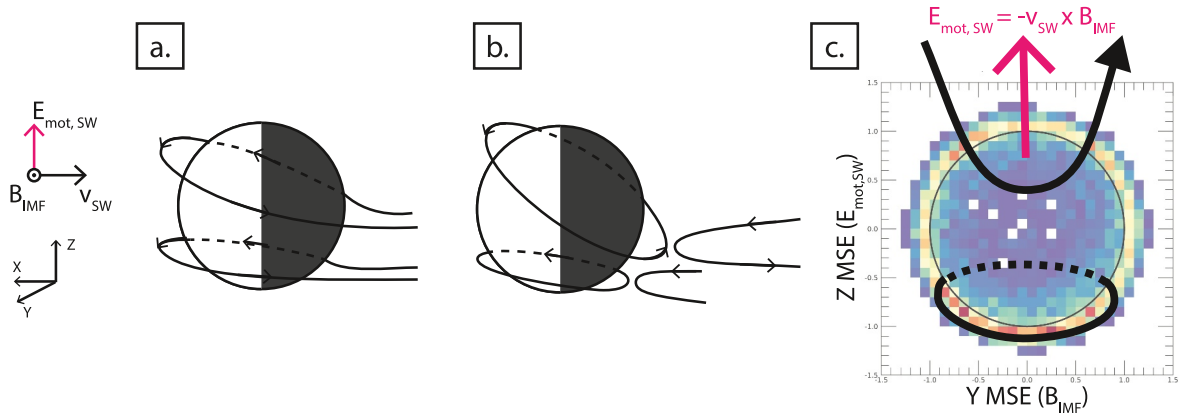


Figure 6. Adapted from Chai et al., 2019. Shows draped and looping magnetic fields and the different orientations of MSE coordinates relative to the physical planet. Final plot is take from Figure 5f, with an overlay of the proposed flux tube configuration in the different $\mathbf{E}_{mot,SW}$ hemispheres.

The locations of the pressure transitions relative to the $\pm E_{mot,SW}$ poles may indicate that mass and energy exchange processes in these regions affect the depth that the IMF can reach within the Martian ionosphere (Dubinin et al., 2014). For example, the outwardly directed solar wind motional electric field creates a "plume" of escaping planetary ions in the $+E_{SW}$ hemisphere, along the $Y_{MSE} \sim 0$ axis (Dong et al., 2015). Also, Shuvalov et al. (2024) found that cold ionospheric plasma is removed near the $+E_{SW}$ pole as the draped magnetic field slides over the planet. The decreased occurrence of pressure transitions at the $+E_{SW}$ pole may indicate that the boundary between an IMF flux tube and the Martian ionosphere is (a) beneath the altitude range used in this study, (b) distorted by the removal of cold ionospheric plasma there, or (c) prevented from being formed (see Figure 5, panel f).

The increase of transition occurrences in the $-E_{SW}$ hemisphere may indicate that the inwardly directed E_{SW} provides the conditions for a barrier, such as a current sheet, to exist between the IMF and the ionosphere. In the next section, we discuss the possible implications of finding more pressure transitions in the $-E_{SW}$ hemisphere.

4.3. Possible Implications of the $\pm E_{SW}$ Asymmetries

A higher density of ionospheric plasma has been shown to exist in the $-E_{SW}$ hemisphere at Mars (Dubinin, Modolo, et al., 2019). This may explain the asymmetries of pressure transitions between the $\pm E_{mot,SW}$ poles shown in Figure 5f because a boundary, such as a current sheet, can be formed between the IMF and Martian ionosphere in the denser $-E_{SW}$ hemisphere.

Within the induced magnetosphere of Venus, Zhang et al. (2010) found that the IMF lines were able to penetrate further into the planet's ionosphere in the $-E_{SW}$ hemisphere. They also found that the field lines become more wrapped in the $-E_{SW}$ hemisphere compared to the $+E_{SW}$ hemisphere. This preferentially forms a magnetic reversal region in the $-E_{SW}$ hemisphere that may lead to reconnection events in the near Venus tail (Xu et al., 2024). The findings of this study indicate that the IMF is also more likely to penetrate into the altitude range studied in the $-E_{SW}$ hemisphere at Mars, which may have similar implications to the findings at Venus.

Reconnection signatures have been observed in the magnetotails of Venus and Mars (see for example, Zhang et al. (2012) and Harada et al. (2015)). Reconnection drives a change in the magnetic field topology that reconfigures ionospheric flows and densities. A release of energy would be expected to accompany reconnection events, especially if the event disrupts currents within the system. A recent study by Lillis et al. (2024) found an auroral signature that appears to be related to the interaction of the draped IMF with the Martian ionosphere, where electron energization processes occur in the Martian-induced magnetotail. Future studies may compare observations of pressure balance locations to auroral events to determine if there is a connection.

Chai et al. (2016, 2019) hypothesized that reconnection events in the induced magnetotail could cause "global looping magnetic fields" to form around Mars and Venus. Figure 6 depicts the proposed global looping field configuration in MSE coordinates and its possible relation to this study. Panel (a) of Figure 6 shows two IMF flux tubes in the positive and negative $E_{mot,SW}$ hemispheres draped around Mars. Panel (b) depicts the global looping fields in both $E_{mot,SW}$ hemispheres after a reconnection event occurs in the magnetotail. Panel (c) shows a 2D

histogram of the observed pressure transition locations in MSE coordinates with the proposed magnetic configuration in both $E_{mot,SW}$ hemispheres overlayed in black lines. Assuming the pressure transition regions studied here mark the depth of IMF penetration into the Martian ionosphere, their statistical locations may show the IMF's usual structure within the ionosphere. In the $+E_{mot,SW}$ hemisphere, a cross-section of a flux tube may be seen off the electric field pole. In the $-E_{mot,SW}$ hemisphere, the even distribution of pressure transitions may suggest the presence of a global looping field.

5. Summary and Conclusion

When the solar wind interacts with a planet with a conductive ionosphere, induced currents are developed that divert solar wind particles around the system at a stand-off point. The magnetic field connected on either side to the unperturbed solar wind can penetrate deeper than this standoff location before sliding over the conducting obstacle. Based on magnetohydrodynamic theory, this study investigates how deep the IMF-associated magnetic field can reach by evaluating the location where the dominant pressure switches from magnetic to thermal ionospheric pressure.

This work has statistically examined the locations where this pressure balance occurs at Mars using observations from the MAVEN mission. These locations were analyzed from a lower altitude of 200 km, below which ions usually become demagnetized, up to an altitude of 800 km, where the pileup boundary is usually found on the dayside. The created database only includes the orbits where thermal observations were made throughout this altitude range. The following assumptions were made in analyzing the pressure transition regions: (a) the inbound/outbound orbit trajectories between 200 and 800 km describe a vertical altitude profile, (b) all pressure is directed radially, and (c) any dynamic, non-equilibrium effects are ignored.

From the database of 14,145 viable orbit segments, we were able to study the statistical structure of pressure balance locations and the conditions that produced an observed pressure balance region. Roughly 45% of the orbits with magnetic pressure dominating at high altitudes did not have a detected transition in the dominant plasma pressure; that is, magnetic pressure dominated throughout the 200–800 km altitude range. These orbits were more likely to occur with more active solar wind conditions (see Figure 2, panels a–c) and they tended to have a periapsis location in the $+E_{SW,mot}$ hemisphere (Figure 2d) and/or over the strong crustal fields (Figure 3b).

In the other 55% of orbits with magnetic pressure dominating at high altitudes, a transition region was detected. These detected transitions were more likely to be found:

1. In the northern hemisphere of the planet, away from the strong crustal fields (Figure 3).
2. At higher altitudes with increasing SZA (Figure 4), and
3. On the dusk side of the planet compared to the dawn side (Figure 4).
4. Near the terminator (Figure 5).
5. In the $-E_{SW,mot}$ hemisphere, and away from the $+E_{SW,mot}$ pole (Figures 2 and 5).

These findings indicate that these transition regions may be driven both by the solar wind and planetary ionospheric conditions. For example, the heightened altitudes of the transitions with increasing SZA mimic what is expected of draped IMF within the induced magnetosphere. Also, the thermosphere is expanded on the dusk side compared to the dawn side due to the rotation of the planet, which is observed in the increased occurrences of transitions near the dusk side in the studied altitude range. Furthermore, the asymmetries between the $\pm E_{mot,SW}$ poles found by mapping the pressure balance regions in MSE coordinates supports the assumption that these regions mark where penetrated IMF interact with the planetary ionosphere.

This study on locations of pressure balance creates a blueprint for where penetrated IMF flux tubes may interact with and influence the Martian ionosphere. Identifying pressure balance locations fundamentally assumes a quasi-static state of the planetary system and the other assumptions mentioned in the introduction. The hybrid magnetosphere of Mars and its interaction with the solar wind causes the system to usually be dynamic. Nevertheless, this study shows that statistical analysis of locations of pressure balance reveals the typical configuration of the penetrated IMF within the ionosphere. This can inform future research focused on understanding the direct interactions between the two plasma regimes.

Data Availability Statement

The research described in this manuscript utilizes publicly available data from the MAVEN mission, including data from the MAG (Connerney, 2024), LPW (Andersson, 2024), and EUV (Eparvier, 2022) instruments. All data were processed using the publicly available SPEDAS software (Angelopoulos et al., 2019). The MAVEN data used in this study are available through the Planetary Data System https://pds-ppi.igpp.ucla.edu/mission/MAVEN (NASA Planetary Data System (PDS), MAVEN Mission [Dataset], 2024). The upstream solar wind data can be accessed at https://homepage.physics.uiowa.edu/~jhalekas/drivers.html (J. Halekas, 2017). The crustal magnetic field model from Langlais et al. (2019) can be generated using the MAVEN IDL Toolkit found at https://lasp.colorado.edu/maven/sdc/public/pages/software.html (MAVEN IDL Toolkit [Software], 2019). The software used and resulting data set can be found on Zenodo at https://doi.org/10.5281/zenodo.14037260 and S.R. Shaver's GitHub repository at https://github.com/spaceskyentist/MAVEN_Pressure_Balance (Shaver, 2024). The authors are unaware of any real or perceived conflicts of interest regarding this study.

Acknowledgments
We acknowledge NASA and the MAVEN mission for support partially through Grant NNH10CC04C to the University of Colorado and by subcontract to Space Sciences Laboratory, University of California, Berkeley. The authors would like to express their gratitude to the two anonymous reviewers for their invaluable discussions, time, and effort in enhancing this work.

References

Acuña, M. H., Connerney, J. E. P., Wasilewski, P., Lin, R. P., Anderson, K. A., Carlson, C. W., et al. (1998). Magnetic field and plasma observations at Mars: Initial results of the Mars global surveyor mission. *Science*, *279*(5357), 1676–1680. https://doi.org/10.1126/science.279.5357.1676

Akbari, H., Andersson, L., Peterson, W. K., Espley, J., Benna, M., & Ergun, R. (2019). Ambipolar electric field in the Martian ionosphere: MAVEN measurements. *Journal of Geophysical Research: Space Physics*, *124*(6), 4518–4524. https://doi.org/10.1029/2018ja026325

Andersson, L. (2024). MAVEN LPW bundle [Dataset]. https://doi.org/10.17189/z5ec-5p12

Andersson, L., Ergun, R. E., Delory, G. T., Eriksson, A., Westfall, J., Reed, H., et al. (2015). The Langmuir Probe and Waves (LPW) Instrument for MAVEN. *Space Science Reviews*, *195*(1–4), 173–198. https://doi.org/10.1007/s11214-015-0194-3

Angelopoulos, V., Cruce, P., Drozdov, A., Grimes, E. W., Hatzigeorgiu, N., King, D. A., et al. (2019). The Space Physics Environment Data Analysis System (SPEDAS). *Space Science Reviews*, *215*(1), 9. https://doi.org/10.1007/s11214-018-0576-4

Baumjohann, W., Blanc, M., Fedorov, A., & Glassmeier, K.-H. (2010). Current systems in planetary magnetospheres and ionospheres. In U. R. Christensen, A. Balogh, D. Breuer, & K.-H. Glaßmeier (Eds.), *Planetary magnetism* (pp. 99–134). Springer New York. https://doi.org/10.1007/978-1-4419-5901-0_4

Bertucci, C., Duru, F., Edberg, N., Fraenz, M., Martinecz, C., Szego, K., & Vaisberg, O. (2011). The induced magnetospheres of Mars, Venus, and titan. *Space Science Reviews*, *162*(1), 113–171. https://doi.org/10.1007/s11214-011-9845-1

Bertucci, C., Mazelle, C., Acuña, M. H., Russell, C. T., & Slavin, J. A. (2005). Structure of the magnetic pileup boundary at Mars and Venus. *Journal of Geophysical Research*, *110*(A1), A01209. https://doi.org/10.1029/2004ja010592

Bougher, S. W., Brain, D. A., Fox, J. L., Francisco, G.-G., Simon-Wedlund, C., Withers, P. G., et al. (2017). Upper neutral atmosphere and ionosphere. In *The atmosphere and climate of mars* (pp. 433–463). Cambridge University Press. https://doi.org/10.1017/9781139060172.014

Bougher, S. W., Engel, S., Roble, R. G., & Foster, B. (1999). Comparative terrestrial planet thermospheres: 2. Solar cycle variation of global structure and winds at equinox. *Journal of Geophysical Research*, *104*(E7), 16591–16611. https://doi.org/10.1029/1998je001019

Brain, D. A., Bagenal, F., Acuna, M. H., & P, C. J. E. (2003). Martian magnetic morphology: Contributions from the solar wind and crust. *Journal of Geophysical Research*, *108*(A12), 1424. https://doi.org/10.1029/2002ja009482

Brain, D. A., Barabash, S., Bougher, S. W., Duru, F., Jakosky, B. M., & Modolo, R. (2017). Solar wind interaction and atmospheric escape. In *The atmosphere and climate of Mars* (pp. 464–496). Cambridge University Press. https://doi.org/10.1017/9781139060172.015

Breus, T. K., Krymskii, A. M., Lundin, R., Dubinin, E. M., Luhmann, J. G., Yeroshenko, Y. G., et al. (1991). The solar wind interaction with Mars: Consideration of phobos 2 mission observations of an ion composition boundary on the dayside. *Journal of Geophysical Research*, *96*(A7), 11165–11174. https://doi.org/10.1029/91ja01131

Chai, L., Wan, W., Wei, Y., Zhang, T., Exner, W., Fraenz, M., et al. (2019). The induced global looping magnetic field on mars. *The Astrophysical Journal Letters*, *871*(2), L27. https://doi.org/10.3847/2041-8213/aaff6e

Chai, L., Wei, Y., Wan, W., Zhang, T., Rong, Z., Fraenz, M., et al. (2016). An induced global magnetic field looping around the magnetotail of Venus. *Journal of Geophysical Research: Space Physics*, *121*(1), 688–698. https://doi.org/10.1002/2015ja021904

Chen, R. H., Cravens, T. E., & Nagy, A. F. (1978). The Martian ionosphere in light of the Viking observations. *Journal of Geophysical Research*, *83*(A8), 3871–3876. https://doi.org/10.1029/JA083iA08p03871

Chu, F., Girazian, Z., Duru, F., Ramstad, R., Halekas, J., Gurnett, D. A., et al. (2021). The dayside ionopause of mars: Solar wind interaction, pressure balance, and comparisons with Venus. *Journal of Geophysical Research: Planets*, *126*(11), e2021JE006936. https://doi.org/10.1029/2021je006936

Chu, F., Girazian, Z., Gurnett, D., Morgan, D., Halekas, J., & Kopf, A. (2019). Observations of the dayside Martian ionopause by the mars express radar sounder. In *Geophysical research abstracts* (Vol. 21). Retrieved from https://search.ebscohost.com/login.aspx?direct=true&profile=ehost&scope=site&authtype=crawler&jrnl=10297006&AN=140493386&h=D5c5rTkLvstWMu1VcuRZ1Sv7eqA6Amf%2F6%2FJqhn6%2BGiLY3uW7QeQ9YVKC3PqKjT15sZpdFVkhw7u2icBDyZyDdg%3D%3D&crl=c

Cloutier, P. A., & Daniell, R. E. (1973). Ionospheric currents induced by solar wind interaction with planetary atmospheres. *Planetary and Space Science*, *21*(3), 463–474. https://doi.org/10.1016/0032-0633(73)90043-3

Connerney, J. E. P. (2024). MAVEN MAG bundle [Dataset]. https://doi.org/10.17189/1414178

Connerney, J. E. P., Acuña, M. H., Ness, N. F., Spohn, T., & Schubert, G. (2004). Mars crustal magnetism. *Space Science Reviews*, *111*(1), 1–32. https://doi.org/10.1023/B:SPAC.0000032719.40094.1d

Connerney, J. E. P., Espley, J., Lawton, P., Murphy, S., Odom, J., Oliversen, R., & Sheppard, D. (2015). The MAVEN magnetic field investigation. *Space Science Reviews*, *195*(1), 257–291. https://doi.org/10.1007/s11214-015-0169-4

Cravens, T. E. (1997). *Physics of solar system plasmas*. Cambridge University Press. Retrieved from https://play.google.com/store/books/details?id=kiB0QgAACAAJ

Cravens, T. E., Hamil, O., Houston, S., Bougher, S., Ma, Y., Brain, D., & Ledvina, S. (2017). Estimates of ionospheric transport and ion loss at mars. *Journal of Geophysical Research: Space Physics*, *122*(10), 10626–10637. https://doi.org/10.1002/2017ja024582

Cravens, T. E., Hamil, O., Renzaglia, A., Ledvina, S. A., & Howard, S. K. (2023). Fourier analysis of magnetic fields in the ionosphere of Mars. *Journal of Geophysical Research: Space Physics*, *128*(4), e2022JA031044. https://doi.org/10.1029/2022ja031044

Crider, D. H., Acuña, M. H., Connerney, J. E. P., Vignes, D., Ness, N. F., Krymskii, A. M., et al. (2002). Observations of the latitude dependence of the location of the Martian magnetic pileup boundary. *Geophysical Series*, *29*(8), 11-1–11-4. https://doi.org/10.1029/2001GL013860

Crider, D. H., Vignes, D., Krymskii, A. M., Breus, T. K., Ness, N. F., Mitchell, D. L., et al. (2003). A proxy for determining solar wind dynamic pressure at mars using mars global surveyor data. *Journal of Geophysical Research*, *108*(A12), 1461. https://doi.org/10.1029/2003ja009875

Dong, Y., Fang, X., Brain, D. A., Hurley, D. M., Halekas, J. S., Espley, J. R., et al. (2019). Magnetic field in the Martian magnetosheath and the application as an IMF clock angle proxy. *Journal of Geophysical Research: Space Physics*, *124*(6), 4295–4313. https://doi.org/10.1029/2019ja026522

Dong, Y., Fang, X., Brain, D. A., McFadden, J. P., Halekas, J. S., Connerney, J. E., et al. (2015). Strong plume fluxes at mars observed by MAVEN: An important planetary ion escape channel. *Geophysical Research Letters*, *42*(21), 8942–8950. https://doi.org/10.1002/2015gl065346

Dubinin, E., Fraenz, M., Pätzold, M., Tellmann, S., Modolo, R., DiBraccio, G., et al. (2023). Magnetic fields and plasma motions in a hybrid Martian magnetosphere. *Journal of Geophysical Research: Space Physics*, *128*(1). https://doi.org/10.1029/2022ja030575

Dubinin, E., Fraenz, M., Pätzold, M., Woch, J., McFadden, J., Halekas, J. S., et al. (2019). Expansion and shrinking of the Martian topside ionosphere. *Journal of Geophysical Research: Space Physics*, *124*(11), 9725–9738. https://doi.org/10.1029/2019ja027077

Dubinin, E., Fraenz, M., Zhang, T. L., Woch, J., & Wei, Y. (2014). Magnetic fields in the mars ionosphere of a noncrustal origin: Magnetization features. *Geophysical Research Letters*, *41*(18), 6329–6334. https://doi.org/10.1002/2014gl061453

Dubinin, E., Modolo, R., Fraenz, M., Päetzold, M., Woch, J., Chai, L., et al. (2019). The induced magnetosphere of Mars: Asymmetrical topology of the magnetic field lines. *Geophysical Research Letters*, *46*(22), 12722–12730. https://doi.org/10.1029/2019gl084387

Dubinin, E., Sauer, K., Lundin, R., Norberg, O., Trotignon, J., Schwingenschuh, K., et al. (1996). Plasma characteristics of the boundary layer in the Martian magnetosphere. *Journal of Geophysical Research*, *101*(A12), 27061–27075. https://doi.org/10.1029/96JA02021

Duru, F., Gurnett, D. A., Frahm, R. A., Winningham, J. D., Morgan, D. D., & Howes, G. G. (2009). Steep, transient density gradients in the Martian ionosphere similar to the ionopause at Venus. *Journal of Geophysical Research*, *114*(A12), A12310. https://doi.org/10.1029/2009ja014711

Eparvier, F. (2022). MAVEN EUV modeled data bundle [Dataset]. https://doi.org/10.17189/1517691

Forbes, J. M., & Moudden, Y. (2009). Solar terminator wave in a mars general circulation model. *Geophysical Research Letters*, *36*(17), L17201. https://doi.org/10.1029/2009gl039528

Fowler, C. M., Shaver, S., Hanley, K. G., Andersson, L., McFadden, J., Mitchell, D., et al. (2024). Disappearing solar wind at Mars: Changes in the mars-solar wind interaction. *Journal of Geophysical Research: Space Physics*, *129*(1), e2023JA031910. https://doi.org/10.1029/2023ja031910

Gao, J. W., Rong, Z. J., Klinger, L., Li, X. Z., Liu, D., & Wei, Y. (2021). A spherical harmonic Martian crustal magnetic field model combining data sets of MAVEN and MGS. *Earth and Space Science*, *8*(10), e2021EA001860. https://doi.org/10.1029/2021ea001860

Girazian, Z., Halekas, J., Morgan, D. D., Kopf, A. J., Gurnett, D. A., & Chu, F. (2019). The effects of solar wind dynamic pressure on the structure of the topside ionosphere of Mars. *Geophysical Research Letters*, *46*(15), 8652–8662. https://doi.org/10.1029/2019gl083643

Gupta, N., Venkateswara Rao, N., & Kadhane, U. R. (2019). Dawn-dusk asymmetries in the Martian upper atmosphere. *Journal of Geophysical Research: Planets*, *124*(12), 3219–3230. https://doi.org/10.1029/2019je006151

Halekas, J. (2017). MAVEN solar wind data [Dataset]. *MAVEN*. Retrieved from https://homepage.physics.uiowa.edu/~jhalekas/drivers.html

Halekas, J. S., McFadden, J. P., Brain, D. A., Luhmann, J. G., DiBraccio, G. A., Connerney, J. E. P., et al. (2018). Structure and variability of the Martian ion composition boundary layer. *Journal of Geophysical Research: Space Physics*, *123*(10), 8439–8458. https://doi.org/10.1029/2018ja025866

Halekas, J. S., Ruhunusiri, S., Harada, Y., Collinson, G., Mitchell, D. L., Mazelle, C., et al. (2017). Structure, dynamics, and seasonal variability of the Mars-solar wind interaction: MAVEN solar wind ion analyzer in-flight performance and science results. *Journal of Geophysical Research: Space Physics*, *122*(1), 547–578. https://doi.org/10.1002/2016ja023167

Halekas, J. S., Shaver, S., Azari, A. R., Fowler, C. M., Ma, Y., Xu, S., et al. (2023). The day the solar wind disappeared at Mars. *Journal of Geophysical Research: Space Physics*, *128*(12), e2023JA031935. https://doi.org/10.1029/2023ja031935

Hamil, O., Cravens, T. E., Rahmati, A., Connerney, J. E. P., & Andersson, L. (2019). Pressure gradients driving ion transport in the topside Martian atmosphere. *Journal of Geophysical Research: Space Physics*, *124*(7), 6117–6126. https://doi.org/10.1029/2019ja026670

Hamil, O., Cravens, T. E., Renzaglia, A., & Andersson, L. (2022). Small scale magnetic structure in the induced Martian ionosphere and lower magnetic pile-up region. *Journal of Geophysical Research: Space Physics*, *127*(4), e2021JA030139. https://doi.org/10.1029/2021ja030139

Han, X., Fraenz, M., Dubinin, E., Wei, Y., Andrews, D. J., Wan, W., et al. (2014). Discrepancy between ionopause and photoelectron boundary determined from Mars express measurements. *Geophysical Research Letters*, *41*(23), 8221–8227. https://doi.org/10.1002/2014GL062287

Harada, Y., Halekas, J. S., McFadden, J. P., Mitchell, D. L., Mazelle, C., Connerney, J. E. P., et al. (2015). Magnetic reconnection in the near-Mars magnetotail: MAVEN observations. *Geophysical Research Letters*, *42*(21), 8838–8845. https://doi.org/10.1002/2015gl065004

Holmberg, M. K. G., André, N., Garnier, P., Modolo, R., Andersson, L., Halekas, J., et al. (2019). MAVEN and MEX multi-instrument study of the dayside of the Martian induced magnetospheric structure revealed by pressure analyses. *Journal of Geophysical Research: Space Physics*, *124*(11), 8564–8589. https://doi.org/10.1029/2019ja026954

Jain, S. K., Soto, E., Evans, J. S., Deighan, J., Schneider, N. M., & Bougher, S. W. (2023). Thermal structure of Mars' middle and upper atmospheres: Understanding the impacts of dynamics and solar forcing. *Icarus*, *393*(114703), 114703. https://doi.org/10.1016/j.icarus.2021.114703

Jakosky, B., Lin, R. P., Grebowsky, J. M., Luhmann, J. G., Mitchell, D. F., Beutelschies, G., et al. (2015). The Mars atmosphere and volatile evolution (MAVEN) mission. *Space Science Reviews*, *195*(1), 3–48. https://doi.org/10.1007/s11214-015-0139-x

Langlais, B., Purucker, M. E., & Mandea, M. (2004). Crustal magnetic field of Mars. *Journal of Geophysical Research*, *109*(E2), 1431. https://doi.org/10.1029/2003je002048

Langlais, B., Thébault, E., Houliez, A., Purucker, M. E., & Lillis, R. J. (2019). A new model of the crustal magnetic field of Mars using MGS and MAVEN. *Journal of Geophysical Research: Planets*, *124*(6), 1542–1569. https://doi.org/10.1029/2018JE005854

Lillis, R. J., Deighan, J., Chirakkil, K., Jain, S., Fillingim, M., Chaffin, M., et al. (2024). Sinuous aurora at Mars: A link to the tail current sheet? *Journal of Geophysical Research: Space Physics*, *129*(6). https://doi.org/10.1029/2024ja032477

Lillis, R. J., Fillingim, M. O., Ma, Y., Gonzalez-Galindo, F., Forget, F., Johnson, C. L., et al. (2019). Modeling wind-driven ionospheric dynamo currents at Mars: Expectations for InSight magnetic field measurements. *Geophysical Research Letters*, *46*(10), 5083–5091. https://doi.org/10.1029/2019GL082536

Luhmann, J. G., & Cravens, T. E. (1991). Magnetic fields in the ionosphere of Venus. *Space Science Reviews*, *55*(1), 201–274. https://doi.org/10.1007/BF00177138

Luhmann, J. G., Ledvina, S. A., & Russell, C. T. (2004). Induced magnetospheres. *Advances in Space Research*, *33*(11), 1905–1912. https://doi.org/10.1016/j.asr.2003.03.031

Ma, Y., Fang, X., Russell, C. T., Nagy, A. F., Toth, G., Luhmann, J. G., et al. (2014). Effects of crustal field rotation on the solar wind plasma interaction with Mars. *Geophysical Research Letters*, *41*(19), 6563–6569. https://doi.org/10.1002/2014gl060785

Ma, Y., Nagy, A. F., Sokolov, I. V., & Hansen, K. C. (2004). Three-dimensional, multispecies, high spatial resolution MHD studies of the solar wind interaction with Mars. *Journal of Geophysical Research*, *109*(A7), A07211. https://doi.org/10.1029/2003ja010367

Marquette, M. L., Lillis, R. J., Halekas, J. S., Luhmann, J. G., Gruesbeck, J. R., & Espley, J. R. (2018). Autocorrelation study of solar wind plasma and IMF properties as measured by the MAVEN spacecraft. *Journal of Geophysical Research: Space Physics*, *123*(4), 2493–2512. https://doi.org/10.1002/2018ja025209

Matsunaga, K., Seki, K., Brain, D. A., Hara, T., Masunaga, K., Mcfadden, J. P., et al. (2017). Statistical study of relations between the induced magnetosphere, ion composition, and pressure balance boundaries around Mars based on MAVEN observations. *Journal of Geophysical Research: Space Physic*, *122*(9), 9723–9737. https://doi.org/10.1002/2017JA024217

MAVEN IDL toolkit. (2019). MAVEN IDL toolkit [Software]. *MAVEN*. Retrieved from https://lasp.colorado.edu/maven/sdc/public/pages/software.html

Mendillo, M., Narvaez, C., Vogt, M. F., Mayyasi, M., Mahaffy, P., Benna, M., et al. (2017). MAVEN and the total electron content of the Martian ionosphere. *Journal of Geophysical Research: Space Physics*, *122*(3), 3526–3537. https://doi.org/10.1002/2016ja023474

Mitchell, D. L., Lin, R. P., Mazelle, C., Rème, H., Cloutier, P. A., Connerney, J. E. P., et al. (2001). Probing Mars' crustal magnetic field and ionosphere with the MGS electron reflectometer. *Journal of Geophysical Research*, *106*(E10), 23419–23427. https://doi.org/10.1029/2000je001435

Moses, S. L., Coroniti, F. V., & Scarf, F. L. (1988). Expectations for the microphysics of the mars-solar wind interaction. *Geophysical Research Letters*, *15*(5), 429–432. https://doi.org/10.1029/gl015i005p00429

Nagy, A. F., Winterhalter, D., Sauer, K., Cravens, T. E., Brecht, S., Mazelle, C., et al. (2004). The plasma environment of Mars. *Space Science Reviews*, *111*(1), 33–114. https://doi.org/10.1023/B:SPAC.0000032718.47512.92

NASA planetary data system (PDS), MAVEN mission. (2024). NASA planetary data system (PDS), MAVEN mission [Dataset]. *NASA*. Retrieved from https://pds-ppi.igpp.ucla.edu/mission/MAVEN

Pérez-de Tejada, H. (1986). Distribution of plasma and magnetic fluxes in the Venus near wake. *Journal of Geophysical Research*, *91*(A7), 8039–8044. https://doi.org/10.1029/JA091iA07p08039

Pilinski, M., Andersson, L., Fowler, C., Peterson, W. K., Thiemann, E., & Elrod, M. K. (2019). Electron temperature response to solar forcing in the low-latitude Martian ionosphere. *Journal of Geophysical Research: Planets*, *124*(11), 3082–3094. https://doi.org/10.1029/2019je006090

Pilinski, M., Bougher, S., Greer, K., Thiemann, E., Andersson, L., Benna, M., & Elrod, M. (2018). First evidence of persistent nighttime temperature structures in the neutral thermosphere of Mars. *Geophysical Research Letters*, *45*(17), 8819–8825. https://doi.org/10.1029/2018gl078761

Pilinski, M. D., Roeten, K. J., Bougher, S. W., & Benna, M. (2023). Dynamical heating in the Martian thermosphere. *Journal of Geophysical Research: Planets*, *128*(6), e2022JE007670. https://doi.org/10.1029/2022je007670

Ramstad, R., Brain, D. A., Dong, Y., Espley, J., Halekas, J., & Jakosky, B. (2020). The global current systems of the Martian induced magnetosphere. *Nature Astronomy*, *4*(10), 979–985. https://doi.org/10.1038/s41550-020-1099-y

Sakai, S., Andersson, L., Cravens, T. E., Mitchell, D. L., Mazelle, C., Rahmati, A., et al. (2016). Electron energetics in the Martian dayside ionosphere: Model comparisons with MAVEN data. *Journal of Geophysical Research: Space Physics*, *121*(7), 7049–7066. https://doi.org/10.1002/2016ja022782

Sánchez-Cano, B., Narvaez, C., Lester, M., Mendillo, M., Mayyasi, M., Holmstrom, M., et al. (2020). Mars' ionopause: A matter of pressures. *Journal of Geophysical Research: Space Physics*, *125*(9), e2020JA028145. https://doi.org/10.1029/2020ja028145

Schunk, R., & Nagy, A. (2009). *Ionospheres: Physics, plasma physics, and chemistry*. Cambridge University Press. Retrieved from https://play.google.com/store/books/details?id=sCJ8xJGRNYIC

Shaver, S. R. (2024). Dataset and analysis software of locations of pressure balance in the Martian ionosphere by S.R. shaver [Dataset]. https://doi.org/10.5281/zenodo.14037260

Shaver, S. R., Solt, L., Andersson, L., Halekas, J., Jian, L., da Silva, D. E., et al. (2024). The Martian ionospheric response to the co-rotating interaction region that caused the disappearing solar wind event at Mars. *Journal of Geophysical Research: Space Physics*, *129*(3), e2023JA032181. https://doi.org/10.1029/2023ja032181

Shuvalov, S., Andersson, L., Halekas, J. S., Fowler, C. M., Hanley, K. G., & DiBraccio, G. (2024). Ionospheric plasma transported into the Martian magnetosheath. *Geophysical Research Letters*, *51*(6), e2023GL107953. https://doi.org/10.1029/2023gl107953

Slavin, J. A., & Holzer, R. E. (1981). Solar wind flow about the terrestrial planets 1. Modeling bow shock position and shape. *Journal of Geophysical Research*, *86*(A13), 11401–11418. https://doi.org/10.1029/JA086iA13p11401

Slavin, J. A., & Holzer, R. E. (1982). The solar wind interaction with Mars revisited. *Journal of Geophysical Research*, *87*(B12), 10285–10296. https://doi.org/10.1029/jb087ib12p10285

Spreiter, J. R., Summers, A. L., & Rizzi, A. W. (1970). Solar wind flow past nonmagnetic planets—Venus and Mars. *Planetary and Space Science*, *18*(9), 1281–1299. https://doi.org/10.1016/0032-0633(70)90139-X

Szegö, K., Glassmeier, K.-H., Bingham, R., Bogdanov, A., Fischer, C., Haerendel, G., et al. (2000). Physics of mass loaded plasmas. *Space Science Reviews*, *94*(3), 429–671. https://doi.org/10.1023/A:1026568530975

Thiemann, E. M. B., Chamberlin, P. C., Eparvier, F. G., Templeman, B., Woods, T. N., Bougher, S. W., & Jakosky, B. M. (2017). The MAVEN EUVM model of solar spectral irradiance variability at Mars: Algorithms and results. *Journal of Geophysical Research: Space Physics*, *122*(3), 2748–2767. https://doi.org/10.1002/2016ja023512

Trotignon, J. G., Mazelle, C., Bertucci, C., & Acuña, M. H. (2006). Martian shock and magnetic pile-up boundary positions and shapes determined from the phobos 2 and Mars global surveyor data sets. *Planetary and Space Science*, *54*(4), 357–369. https://doi.org/10.1016/j.pss.2006.01.003

Vignes, D., Mazelle, C., Rme, H., Acuña, M. H., Connerney, J. E. P., Lin, R. P., et al. (2000). The solar wind interaction with mars: Locations and shapes of the bow shock and the magnetic pile-up boundary from the observations of the MAG/ER experiment onboard mars global surveyor. *Geophysical Research Letters*, *27*(1), 49–52. https://doi.org/10.1029/1999gl010703

Vogt, M. F., Withers, P., Mahaffy, P. R., Benna, M., Elrod, M. K., Halekas, J. S., et al. (2015). Ionopause-like density gradients in the Martian ionosphere: A first look with MAVEN. *Geophysical Research Letters*, *42*(21), 8885–8893. https://doi.org/10.1002/2015gl065269

Xu, S., Liemohn, M. W., Dong, C., Mitchell, D. L., Bougher, S. W., & Ma, Y. (2016). Pressure and ion composition boundaries at Mars. *Journal of Geophysical Research: Space Physics*, *121*(7), 6417–6429. https://doi.org/10.1002/2016ja022644

Xu, S., Mitchell, D. L., Whittlesey, P., Rahmati, A., Livi, R., Larson, D., et al. (2024). Closed magnetic topology in the Venusian magnetotail and ion escape at Venus. *Nature Communications*, *15*(1), 1–9. https://doi.org/10.1038/s41467-024-50480-0

Xu, S., Weber, T., Mitchell, D. L., Brain, D. A., Mazelle, C., DiBraccio, G. A., & Espley, J. (2019). A technique to infer magnetic topology at Mars and its application to the terminator region. *Journal of Geophysical Research: Space Physics*, *124*(3), 1823–1842. https://doi.org/10.1029/2018ja026366

Zhang, T. L., Baumjohann, W., Du, J., Nakamura, R., Jarvinen, R., Kallio, E., et al. (2010). Hemispheric asymmetry of the magnetic field wrapping pattern in the Venusian magnetotail. *Geophysical Research Letters*, *37*(14), L14202. https://doi.org/10.1029/2010gl044020

Zhang, T. L., Baumjohann, W., Teh, W. L., Nakamura, R., Russell, C. T., Luhmann, J. G., et al. (2012). Giant flux ropes observed in the magnetized ionosphere at Venus. *Geophysical Research Letters*, *39*(23), L23103. https://doi.org/10.1029/2012gl054236